Mast Cell Degranulation Is Accompanied by the Release of a Selective Subset of Extracellular Vesicles That Contain Mast Cell–Specific Proteases

This information is current as of December 15, 2016.

Tom Groot Kormelink, Ger J. A. Arkesteijn, Chris H. A. van de Lest, Willie J. C. Geerts, Soenita S. Goerdayal, Maarten A. F. Altelaar, Frank A. Redegeld, Esther N. M. Nolte-'t Hoen and Marca H. M. Wauben

Supplementary Material	**http://www.jimmunol.org/content/suppl/2016/09/10/jimmunol.160061 4.DCSupplemental.html**
References	This article **cites 75 articles**, 29 of which you can access for free at: http://www.jimmunol.org/content/197/8/3382.full#ref-list-1
Subscriptions	Information about subscribing to *The Journal of Immunology* is online at: http://jimmunol.org/subscriptions
Permissions	Submit copyright permission requests at: http://www.aai.org/ji/copyright.html
Email Alerts	Receive free email-alerts when new articles cite this article. Sign up at: http://jimmunol.org/cgi/alerts/etoc

Mast Cell Degranulation Is Accompanied by the Release of a Selective Subset of Extracellular Vesicles That Contain Mast Cell–Specific Proteases

Tom Groot Kormelink,* Ger J. A. Arkesteijn,*,† Chris H. A. van de Lest,*
Willie J. C. Geerts,‡ Soenita S. Goerdayal,§ Maarten A. F. Altelaar,§ Frank A. Redegeld,¶
Esther N. M. Nolte-'t Hoen,* and Marca H. M. Wauben*

Mast cells (MC) are well known for their effector role in allergic disorders; moreover, they are associated with diverse modulatory effects in innate and adaptive immunity. It is largely unclear how MC exert these modulating functions. In this article, we show that IgE-mediated MC degranulation leads to a rapid release of high quantities of extracellular vesicles (EV), comparable to the release of preformed mediators. EV are submicron structures composed of lipid bilayers, proteins, and nucleic acids that are released by cells in a regulated fashion and are involved in intercellular communication. Primary murine mucosal-type MC and connective tissue–type MC released phenotypically different EV populations depending on the stimulus they received. Although unstimulated MC constitutively released CD9$^+$ EV, degranulation was accompanied by the release of CD63$^+$ EV, which correlated with release of the soluble mediator β-hexosaminidase. This CD63$^+$ EV subset was smaller and exhibited a higher buoyant density and distinct phospholipid composition compared with CD9$^+$ EV. Marked differences were observed for phosphatidylinositol, phosphatidic acid, and bis(monoacylglycero)phosphate species. Strikingly, proteomic analysis of CD63$^+$ EV from connective tissue–type MC unveiled an abundance of MC-specific proteases. With regard to carboxypeptidase A3, it was confirmed that the enzyme was EV associated and biologically active. Our data demonstrate that, depending on their activation status, MC release distinct EV subsets that differ in composition and protease activity and are indicative of differential immunological functions. Concerning the strategic tissue distribution of MC and the presence of degranulated MC in various (allergic) disorders, MC-derived EV should be considered potentially important immune regulators. *The Journal of Immunology*, 2016, 197: 3382–3392.

Mast cells (MC) are granular immune cells located throughout the body at mucosal, submucosal, and connective tissues, especially at sites contacting the external environment, as well as in secondary lymphoid tissues and surrounding blood and lymph vessels (1, 2). In addition to the well-defined effector function of MC in allergic disorders, increasing evidence shows that MC play a prominent role in modulating innate and adaptive immunity and that they are associated with the initiation and progression of multiple immune disorders (reviewed in Refs. 3–5). The mechanisms by which MC exert these effects are poorly defined, although soluble mediator release and direct contact with other immune cells, including dendritic cells and T cells, are likely to be involved (6–10).

Upon activation, MC can release a variety of soluble mediators that are generally categorized as preformed mediators (e.g., histamine, proteases) that are stored in secretory granules, also termed secretory lysosomes; de novo–synthesized lipid mediators; and de novo–synthesized cytokines and chemokines (11). Large quantities of preformed mediators can be released into the extracellular environment within minutes after activation as the result of rapid fusion of secretory granules with the plasma membrane, a process known as degranulation (12). Moreover, certain stimuli (e.g., TLR activation) induce the release of mediators in the absence of degranulation (13, 14).

In addition to soluble mediators, viable cells are able to release extracellular vesicles (EV) that play a role in intercellular communication and induce significant functional effects in different (patho)physiological processes, such as immune responses (15, 16), cancer (17), and cardiovascular diseases (18). EV released by viable cells are small vesicular structures, with the vast majority typically ranging from 50 to 200 nm in size. EV are composed of selected lipids (forming a bilayer membrane), proteins, and

*Department of Biochemistry and Cell Biology, Faculty of Veterinary Medicine, Utrecht University, 3584 CM Utrecht, the Netherlands; †Department of Infectious Diseases and Immunology, Faculty of Veterinary Medicine, Utrecht University, 3584 CL Utrecht, the Netherlands; ‡Biomolecular Imaging, Bijvoet Center, Utrecht University, 3584 CH Utrecht, the Netherlands; §Biomolecular Mass Spectrometry and Proteomics Group, Bijvoet Center for Biomolecular Research and Utrecht Institute for Pharmaceutical Sciences, Utrecht University, 3584 CH Utrecht, the Netherlands; and ¶Division of Pharmacology, Department of Pharmaceutical Sciences, Faculty of Science, Utrecht University, 3584 CG Utrecht, the Netherlands

ORCIDs: 0000-0003-2143-2825 (C.H.A.v.d.L.); 0000-0002-4530-7458 (W.J.C.G.); 0000-0002-7893-8192 (S.S.G.); 0000-0003-0360-0311 (M.H.M.W.).

nucleic acids (19). The composition differs between different cell types and depends on the cellular activation state (20). This selective incorporation of cargo determines where and how EV exert their function. EV are released into the environment by the fusion of endosomal multivesicular bodies with the plasma membrane, resulting in the release of their intraluminal vesicles, or by outward budding from the plasma membrane (19). It is impossible to deduce the biogenesis route of released EV because of the lack of discriminatory markers for the different subsets (21).

MC also release EV, constitutively and after IgE-mediated degranulation (22–27). Interestingly, such EV not only derive from the plasma membrane or multivesicular bodies (27), but probably also from secretory granules (22). In relation to function, MC-derived EV (MC-EV) can transfer RNA species to other MC (28, 29) and can contain lipid mediators (25). Using bone marrow–derived MC and cell lines, it was suggested that MC-EV exert immune-stimulatory effects on dendritic cells, T cells, and B cells (23, 24). Because these earlier studies were performed using 70,000–100,000 × g pellets from culture supernatants, which contain (lipo)protein particles and protein aggregates in addition to EV (30, 31), studies using phenotypically different primary mature MC and state-of-the-art technology to purify and characterize EV subpopulations are needed to further elucidate the release and function of MC-EV.

In this study, we investigated the release and content of MC EV derived from mucosal-type MC (MMC) and connective tissue-type MC (CTMC), which represent the two main murine MC phenotypes (32). EV analyses were performed after differential centrifugation and EV purification by density gradient ultracentrifugation to exclude contamination with (lipo)protein particles or protein aggregates (30, 31). A striking release of high numbers of EV was observed upon degranulation, as quantified using single particle–based high-resolution flow cytometry (33, 34). These EV were distinct from the EV released from nondegranulating MC based on content (proteomics and lipidomics) and morphology (cryo-transmission electron microscopy [TEM]), and they contained functional MC-specific mediators that were previously described as soluble only. Together, these analyses led to the finding that MC, irrespective of their phenotype, release distinct EV subsets depending on their activation status, which, therefore, can have differential immunological roles.

Materials and Methods

MC cultures

MC were generated from 8–12-wk-old C57BL/6 mice. Experiments were approved by the Institutional Ethical Animal Committee at Utrecht University. To obtain CTMC, peritoneal MC (PMC) cultures were performed as described previously, with some modifications (35). Briefly, cells were collected by washing the peritoneal cavity with cold PBS and were cultured in culture medium containing RPMI 1640 + GlutaMAX (Life Technologies, Bleiswijk, the Netherlands) supplemented with 2 mM UltraGlutamine (BioWhittaker, Frederick, MD), 10% heat-inactivated FCS (Sigma-Aldrich, St. Louis, MO), 1 mM pyruvate, 1× nonessential amino acids, 100 IU/ml penicillin and 100 mg/ml streptomycin (all from Life Technologies), 50 μM 2-ME, and 50 ng/ml recombinant mouse IL-4, IL-3, and stem cell factor (ProSpec, Ness-Ziona, Israel). After 1 wk, nonadherent cells were collected and cultured in fresh culture medium. Subsequently, half of the culture medium was refreshed twice weekly, and the cell density of nonadherent cells was kept at 0.35–0.75 × 10^6 cells/ml. Spleen-derived MC (SpMC) were cultured as representatives of MMC as follows: single-cell suspensions were prepared from spleens, followed by RBC lysis using ACK lysis buffer. Cells were washed and resuspended in culture medium, as described above, containing 10 ng/ml IL-3 and stem cell factor. The culture volume was doubled after 1 wk; after 2 wk, half of the culture medium was refreshed twice weekly. Cell density of nonadherent cells was kept at 0.5–1.0 × 10^6 cells/ml. After 4 wk of culture, when the purity of PMC and SpMC was between 90 and 95% (based on expression of c-Kit [CD117] and FcεRI, as assessed by flow cytometry), cells were used for experiments up until 6 wk of culture.

Assays for MC activation

To analyze IgE-mediated MC activation, SpMC and PMC were primed for 1.5 h or overnight with DNP-specific IgE (DNP-IgE), washed once in 1% FCS/RPMI 1640, and incubated with DNP-specific human serum albumin (DNP-HSA; Sigma-Aldrich). Activation by compound 48/80 (c48/80), substance P (SP), or LPS (all from Sigma-Aldrich) was performed on nonprimed cells. Degranulation assays were performed on 0.65 × 10^6 cells/ml in 1% FCS/RPMI 1640 without phenol red. The magnitude of degranulation was assessed by analysis of β-hexosaminidase release. This was quantified by measuring fluorescence with a microplate reader (excitation/emission = 360/460 nm; CLARIOstar; BMG LABTECH) after incubating 50 μl of cell-free supernatant with 50 μl of 152 μM 4-methylumbelliferyl N-acetyl-β-D-glucosaminide (Sigma-Aldrich) in 0.1 M citrate buffer (pH 4.5) for 1 h at 37°C and terminating the reaction by adding 100 μl of 0.2 M glycine (pH 10.7). The percentage of β-hexosaminidase release was calculated by determining the ratio of fluorescence supernatant/fluorescence cell lysate (0.5% Triton X-100 [TX-100] was used for cell lysis) corrected for background fluorescence in nonactivated cells. IL-6 concentrations were determined by a mouse IL-6 ELISA MAX Standard Set (BioLegend, San Diego, CA), according to the manufacturer's instructions.

EV isolation, labeling, and flotation

For overnight EV production, cells were washed in RPMI 1640/1% EV-depleted FCS, resuspended in culture medium (as described above, but using EV-depleted FCS), and cultured at 0.65–0.75 × 10^6 cells/ml. FCS (and BSA) were depleted from EV and protein aggregates by overnight centrifugation of 30% FCS/RPMI 1640 (and 5% BSA/PBS) at 100,000 × g (average) in an SW28 rotor (Beckman Coulter, Fullerton, CA). To analyze EV release after MC activation (e.g., via IgE-cross-linking), the activation assays described above were performed using EV-depleted FCS. The isolation and labeling of EV were performed as described previously (33), with some modifications. Briefly, EV were collected from culture supernatants by differential centrifugation (2 × 10 min at 200 × g, 2 × 10 min at 500 × g, 1 × 10 min at 10,000 × g), followed by a pelleting step at 100,000 × g (average) for 65 min in an SW40 rotor (Beckman Coulter). The 10,000 × g pelleting step is crucial when investigating supernatants from degranulated MC, because these pellets contain proteoglycan-containing cores that remain after dissociation of soluble mediators, also known as granule remnants (36–39). When performing sucrose gradients, pelleted EV were resuspended in 20 μl of PBS/0.2% ultracentrifuged BSA (UC-BSA) containing 0.5 μg fluorochrome-labeled anti-mouse CD9 Ab (KMC8; BioLegend) and CD63 Ab (NVG-2; eBioscience, San Diego, CA) or with similarly labeled isotype controls and incubated for 60 min at room temperature. Subsequently, EV were labeled with 7.5 μM PKH67 (Sigma-Aldrich) in 200 μl for 3 min and mixed with 100 μl of 10% EV-depleted FCS (to stop the labeling reaction) and 1.5 ml 2.5 M sucrose. This mixture was overlaid with a linear sucrose gradient (2.0–0.4 M sucrose in PBS) in an SW40 tube and centrifuged for 15–17 h at 192,000 × g (average). One-milliliter gradient fractions were collected from the bottom of the tube. When performing iodixanol gradients, pelleted EV were resuspended in 30 μl of PBS containing 20 μM 5-(and-6)-CFSE (CFDA-SE; Life Technologies) and incubated for 60 min at room temperature. Subsequently, Ab labeling was performed for 60 min by adding 10 μl of PBS/0.8% UC-BSA containing the above mentioned Ab. Then, EV were mixed with 260 μl of PBS/0.05% UC-BSA and 1 ml 60% iodixanol (OptiPrep; Axis-Shield, Oslo, Norway) overlaid with 500 μl of 40% iodixanol, 500 μl of 30% iodixanol, and 1.8 ml of 10% iodixanol and floated into the gradient by centrifugation in an SW60 tube (Beckman Coulter) for 13 h at 192,000 × g (average). Gradient fractions of 250 μl were collected by pipetting from the top of the tube. All densities were determined by refractometry. To pellet floated EV, EV-containing fractions were diluted in PBS/0.1% UC-BSA (sucrose fractions: 4–12×; iodixanol fractions: 50×) and centrifuged at 192,000 × g (average) for 65 min using an SW40 rotor. Selection of sucrose or iodixanol gradients was dependent on the research question; sucrose gradients have the advantage that EV are well separated based on their differences in buoyant density, and iodixanol gradients have the advantage that the majority of EV float into a relatively small volume.

High-resolution flow cytometry of single vesicles

High-resolution flow cytometry of EV was performed on a jet-in-air-based BD Influx flow cytometer (BD Biosciences, San Jose, CA) using an optimized configuration, as previously described in detail (33, 34). In brief, the BD Influx was triggered on the fluorescence signal derived from the fluorescently labeled EV (PHK67 or CFSE), and thresholding was applied on this channel. The threshold level was adjusted to allow an event rate ≤ 10/s when running clean PBS. Forward scatter was measured with a collection angle of 15–25°

(reduced wide-angle forward scatter [rw-FSC]). Three lasers were used: a 200-mW 488-nm laser (Sapphire; Coherent, Santa Clara, CA), an 150-mW 561-nm laser (Jive; Cobolt, Solna, Sweden), and an 120-mW 640-nm laser (Melles Griot, Carlsbad, CA). A large-bore nozzle (140 μm) was used, sheath pressure was permanently monitored and kept within 4.89 to 5.02 psi, and the sample pressure was set at 4.29 psi, to assure an identical diameter of the core in the jet stream. EV counts were determined by measuring each sample for 30 s. Sucrose and iodixanol fractions were diluted 20× and 400× in PBS, respectively, to keep the event rate < 10,000/s to avoid coincident particle detection and occurrence of swarm (40). Yellow-green fluorescent (505/515) polystyrene FluoSpheres beads (Life Technologies) of 100 and 200 nm nominal size were used for calibration of the fluorescence and rw-FSC settings (33).

Cryo-TEM and assessment of EV size distribution

To obtain high EV concentrations, EV were pelleted from culture supernatant, following the above-described protocol, with a final pelleting step at 100,000 × g, resuspended in 20 μl of PBS/0.2% UC-BSA, and used immediately for sample preparation. Sample (3 μl) was placed on the surface of a glow discharged QUANTIFOIL Micromachined Holey Carbon (R 2/2) TEM grid (Quantifoil Micro Tools, Jena, Germany) held by a Vitrobot Mark IV tweezer (FEI, Eindhoven, the Netherlands). The Vitrobot environmental chamber was equilibrated at room temperature and 100% humidity. Blotting conditions were chosen such that a 100–500-nm liquid specimen film spanning holes of the grid was formed when excess water was removed by blotting filter paper. Specimens were released into liquid ethane at its freezing point, where the thin specimen films were vitrified, followed by transfer under liquid nitrogen into a 626 single tilt liquid nitrogen cryo holder (Gatan, Munich, Germany) and into a Tecnai 20 LaB6 electron microscope (FEI), where the specimen temperature was maintained below −165°C. An Eagle 4kX4k CCD camera (FEI) was used under normal and low-dose (nominal under focus of 2 μm) conditions to record images. Pixel EV diameter was measured using IMOD software package 3 (version 4.8.39) and converted to nanometers using calibrated scale bars that were recorded for each individual image.

EV phospholipid analysis by HPLC–mass spectrometry

Lipids were extracted from dried pellets of EV floated into iodixanol gradients, according to the method of Bligh and Dyer (41), with 6 M HCl (0.1% v/v) added to the second chloroform wash to increase recovery of acidic phospholipids. Chromatography was performed on a hydrophilic interaction liquid chromatography column (Phenomenex, Torrance, CA). Approximately 100 pmol of lipid extract in chloroform/methanol (1:1) was injected, followed by elution with a gradient from acetonitrile/acetone (9:1, v/v) to acetonitrile/H_2O (7:3, v/v). Flow rate was 1 ml/min. The column outlet was connected to a heated electrospray ionization source of a linear ion trap mass spectrometer (LTQ-XL, Thermo Scientific, Waltham, MA) and analyzed in negative ion mode. Full-scan spectra were collected in the range of 400 to 950 amu. All solvents were supplied by Biosolve (Valkenswaard, the Netherlands). Data were converted to mzXML format and analyzed using XCMS version 1.32.0 running under R version 2.13.2 (http://www.R-project.org) (42).

EV proteome analysis by high-resolution liquid chromatography–tandem mass spectrometry

Pellets of EV floated into iodixanol gradients were resuspended in nonreducing Laemmli sample buffer, heated at 95°C for 5 min, and separated on a 12% Tris-HCl gel. Gel lanes were excised for in-gel digestion using trypsin and were analyzed essentially as described previously (43). Briefly, samples were analyzed on a Q Exactive Plus instrument (Thermo Scientific, Bremen, Germany) connected to a Proxeon UHPLC (Thermo Scientific, Odense, Denmark) system. For the mass spectrometry analysis, the 10 most intense ions in the survey scan (375–1600 m/z; resolution 35,000; AGC target 3e6) were subjected to higher-energy collisional dissociation fragmentation (resolution 17,500; AGC target 5e4), with the normalized collision energy set to 25% for higher-energy collisional dissociation. Mass spectrometry raw data were processed with Proteome Discoverer (version 1.3; Thermo Scientific); peptide identification was performed using Mascot 2.3 (Matrix Science, London, U.K.), searched against the UniProt database with taxonomy Mus musculus (UniProt, July 2014, 546,121 entries) supplemented with frequently observed contaminants. Two missed cleavages were allowed; carbamidomethylation was set as a fixed modification, and oxidation was set as a variable modification. Data filtering using Percolator software resulted in a 1% false discovery rate. Proteomics data were submitted to Vesiclepedia (www.microvesicles.org), the online community compendium for EV, under accession number Vesiclepedia_575.

Western blot analysis

Cells and pellets of EV that floated into iodixanol gradients were resuspended in nonreducing Laemmli sample buffer. DTT (25 mM) was used to reduce samples when indicated. Samples were heated at 100°C for 5 min and run on 4–20% Criterion TGX gels (Bio-Rad, Hercules, CA) or 10% polyacrylamide gels. After transfer to polyvinylidene difluoride membranes (Immobilon-P; Millipore), the membranes were blocked in PBS containing 5% (w/v) nonfat dry milk powder (Protifar plus; Nutricia, Zoetermeer, the Netherlands) and 0.1% (v/v) Tween-20 and immunolabeled with rat anti-mouse CD9 (KMC8; eBioscience) and rat anti-mouse CD63 (R5G2; MBL, Woburn, MA) under nonreducing conditions. Immunolabeling with anti-mouse Hsc70/Hsp70 (N27F3-4) (both from Enzo Life Sciences, Lausanne, Switzerland), Hsp90 (68/Hsp90; BD Biosciences), carboxypeptidase A3 (CPA3) (H-50; Santa Cruz Biotechnology, Heidelberg, Germany), FcεRI, γ subunit (06-727; Millipore), or CD117 (D13A2; Cell Signaling Technology, Beverly, MA) was performed on reduced samples. HRP-conjugated goat anti-mouse (Jackson ImmunoResearch, Suffolk, U.K.), rabbit anti-rat, goat anti-rabbit (both from Dako), and rabbit anti-goat (Nordic Immunology, Tilburg, the Netherlands) were used as secondary Ab and were detected using SuperSsignal West Dura chemiluminescent substrate (Thermo Scientific). Imaging was performed using a ChemiDoc MP system and Image Lab software (version 5.1; Bio-Rad, Veenendaal, the Netherlands).

Carboxypeptidase A activity assay

To analyze CPA3 activity, EV floated into iodixanol gradients were resuspended in PBS/0.1% UC-BSA. MC were lysed in PBS/2 M NaCl/0.5% TX-100 for 15 min on ice. A 60-μl sample of EV, cell lysate, or culture supernatant was mixed with 40 μl of water and 20 μl of chromogenic substrate (1.8 mM; N-[4-methoxyphenyl-azoformyl]-Phe-OH; Bachem, Bubendorf, Switzerland), after which substrate degradation was monitored for 60 min by measuring the absorbance at OD_{350} with a VersaMax spectrophotometer (Molecular Devices, Sunnyvale, CA) (44, 45).

Results

SpMC and PMC represent mature MMC- and CTMC-like phenotypes

To investigate EV release from the two main murine MC phenotypes, SpMC and PMC were cultured to represent MMC and CTMC, respectively. Flow cytometric analysis showed that both phenotypes were granular, based on side scatter, and expressed CD117 and FcεRI, which is characteristic of MC (Supplemental Fig. 1A, 1B). Alcian blue/safranin staining showed clear blue coloring of SpMC, indicating the presence of the MMC-related proteoglycan chondroitin sulfate, whereas PMC showed intense red granular coloring, indicating the presence of the CTMC-related proteoglycan heparin (45) (Supplemental Fig. 1C, upper panels). Together with the intense toluidine blue staining and lack of abundant vacuoles (Supplemental Fig. 1C, lower panels), this suggested a mature phenotype for these cells. Western blot analysis of cell lysates revealed the presence of CTMC-related proteases CPA3, MC protease (mMCP)4, mMCP5, and mMCP6 in PMC, whereas they were absent or rare in SpMC (Supplemental Fig. 1D). Finally, the functional capacity of PMC, but not SpMC, to degranulate via a G protein–mediated mechanism induced by SP and c48/80 further substantiated their different cellular phenotypes (46, 47) (Supplemental Fig. 1E). Together, this characterization supports the use of SpMC and PMC as model systems for the two main distinct murine MC phenotypes.

Unstimulated and degranulating MC release distinct EV subsets

We analyzed the kinetics of EV release from resting and degranulating MC by high-resolution flow cytometric analysis of individual EV (33, 34). EV were isolated by differential centrifugation, followed by flotation into density gradients. Culture supernatants from degranulating MC were collected 1.5 h after the start of degranulation, the time required for complete degranulation

(Supplemental Fig. 2A). High-resolution flow cytometric analyses of EV in culture supernatants of degranulated MC (IgE-EV) isolated from $10,000 \times g$ pellets indicated the presence of large floating aggregated structures, as shown for PMC IgE-EV (Supplemental Fig. 2B, upper left panel). Likely, these were so-called granule remnants released during degranulation (36–39), because heparinase treatment of the $10,000 \times g$ pellets substantially reduced the number of strong light-scattering particles and resulted in light scatter profiles more similar to single EV (Supplemental Fig. 2B, upper right panel). In contrast, heparinase treatment had no effect on light or fluorescent scatter patterns of IgE-EV isolated from $100,000 \times g$ pellets (Supplemental Fig. 2B, lower panels). Consequently, for the analysis of true MC-EV, we further analyzed only the $100,000 \times g$ pelleted EV. Both MC phenotypes released EV under unstimulated conditions (rest-EV), of which the majority floated at expected sucrose densities of 1.13–1.19 g/ml (Fig. 1A). Notably, the number of rest-EV released by PMC was consistently higher compared with SpMC (mean 2.7-fold difference, $n = 5$, $p = 0.04$). Significantly higher EV numbers were detected in culture supernatants of degranulating MC. Strikingly, the MC supernatants collected 1.5 h after the start of maximal IgE-mediated degranulation contained up to four times more EV compared with supernatants from unstimulated MC harvested after 24 h of culture (mean 2.7-fold difference, $n = 8$,

$p = 0.007$). In contrast to rest-EV, the majority of IgE-EV displayed higher buoyant densities (1.17–1.22 g/ml, Fig. 1A). Consistent differences in light scattering (Fig. 1B, top; side scatter versus rw-FSC) and fluorescence (Fig. 1B, bottom; PKH versus rw-FSC) were observed between rest-EV and IgE-EV for SpMC and PMC. These differences were most obvious when using iodixanol gradients because this resulted in the accumulation of most EV into a small volume. Because differences in buoyant density and light scattering of single EV are indicative of differences in morphology and/or size, cryo-TEM was performed (Fig. 1C). IgE-EV from both MC phenotypes were significantly smaller compared with rest-EV ($p < 0.0001$), and the size distribution of IgE-EV was narrower. Median EV diameters (10th–90th percentile) were SpMC rest-EV: 73 nm (43–249 nm), SpMC IgE-EV: 49 nm (35–73 nm), PMC rest-EV: 144 nm (72–304 nm), and PMC IgE-EV: 53 nm (41–80 nm) (Fig. 1D). Together, these data indicate that degranulating MC rapidly release large quantities of EV that differ in buoyant density and size from EV released by unstimulated MC.

EV derived from unstimulated and degranulated MC differ in CD9 and CD63 content

CD9 and CD63, two commonly used EV markers that are suggested to be present on distinct EV subpopulations (48), were

FIGURE 1. Quantitative and qualitative analysis of EV released by unstimulated and degranulated SpMC and PMC. (**A**) EV from culture supernatants of unstimulated or degranulated (via IgE cross-linking) MC were isolated after a 24- or 1.5-h culture, respectively, stained with PKH67, floated into sucrose density gradients, and quantified by single EV-based high-resolution flow cytometry. Data shown are the number of events recorded in 30 s. (**B**) A similar analysis as described in (A) of CFSE-labeled EV that were floated in iodixanol gradients. Representative dot plots (side scatter [SSC] versus rw-FSC [upper panels]; CFSE versus rw-FSC [lower panels]) of 10,000 SpMC- and PMC-derived rest-EV and IgE-EV that floated at 1.07 g/ml iodixanol. (**C**) Representative cryo-TEM pictures (original magnification ×19,000) of SpMC rest-EV (left panel) and IgE-EV (right panel), obtained from a $100,000 \times g$ pelleting step from culture supernatant (no flotation). (**D**) A size distribution was generated by determining the diameter of ≥200 EV/sample. Lines represent median with interquartile range. Data shown are representative of two independent experiments.
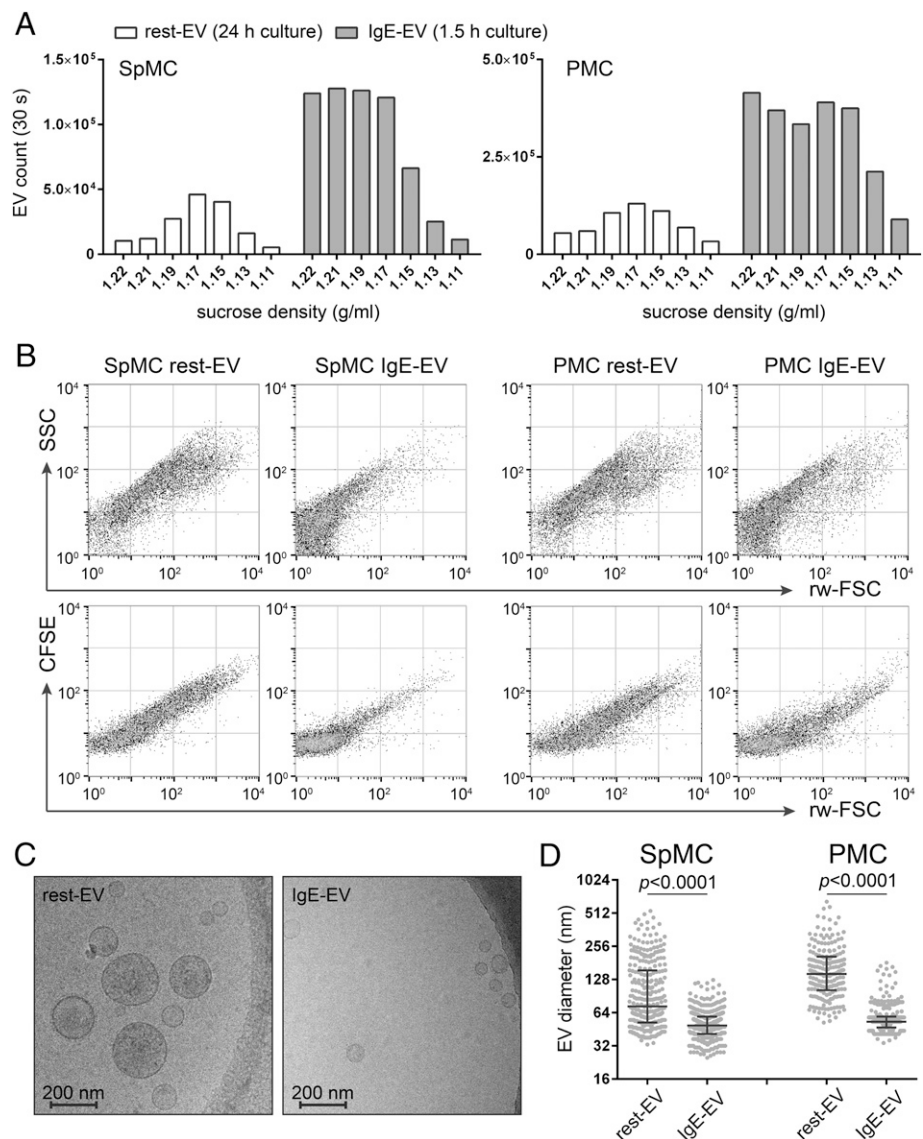
analyzed to further characterize MC-EV. Western blotting showed that rest-EV (sucrose densities 1.13–1.19 g/ml) from SpMC and PMC primarily contained CD9 (Fig. 2A, left). PMC rest-EV also contained some CD63, which was detected in similar fractions as CD9. In contrast to rest-EV, SpMC and PMC IgE-EV contained high levels of CD63, especially in high-density sucrose fractions (between 1.19 and 1.22 g/ml; Fig. 2A, right). Additionally, SpMC IgE-EV contained substantial levels of CD9, comparable to rest-EV. To further validate the presence of CD9 and CD63 on different EV subsets, we used high-resolution flow cytometric analysis of EV stained with fluorescently labeled Abs. Rest-EV from both MC phenotypes were mostly single positive for CD9 (Fig. 2B, 2C), whereas PMC IgE-EV were mostly single positive for CD63 (Fig. 2B, 2C). SpMC IgE-EV appeared to be CD63 single positive at high densities; however, at lower densities, CD9 single-positive EV and CD63/CD9 double-positive EV were also observed

(Fig. 2B, 2C). Altogether, these results indicate that EV derived from unstimulated and degranulating MC differ in buoyant density and size, as well as in their CD9 and CD63 content.

EV release correlates with soluble mediator release upon degranulation

Thus far, we analyzed IgE-EV that were released within 1.5 h after start of degranulation at optimal conditions. To investigate whether the observed rapid EV release was dependent on the duration, strength, and type of degranulating stimulus, we next performed time-course experiments and induced degranulation by incubating IgE-primed MC with different concentrations of DNP-HSA, c48/80, or SP. The latter two are known secretagogues that induce degranulation of only CTMC via an IgE-independent mechanism (49). For both MC phenotypes, the total number of EV released after degranulation strongly correlated with the time-dependent
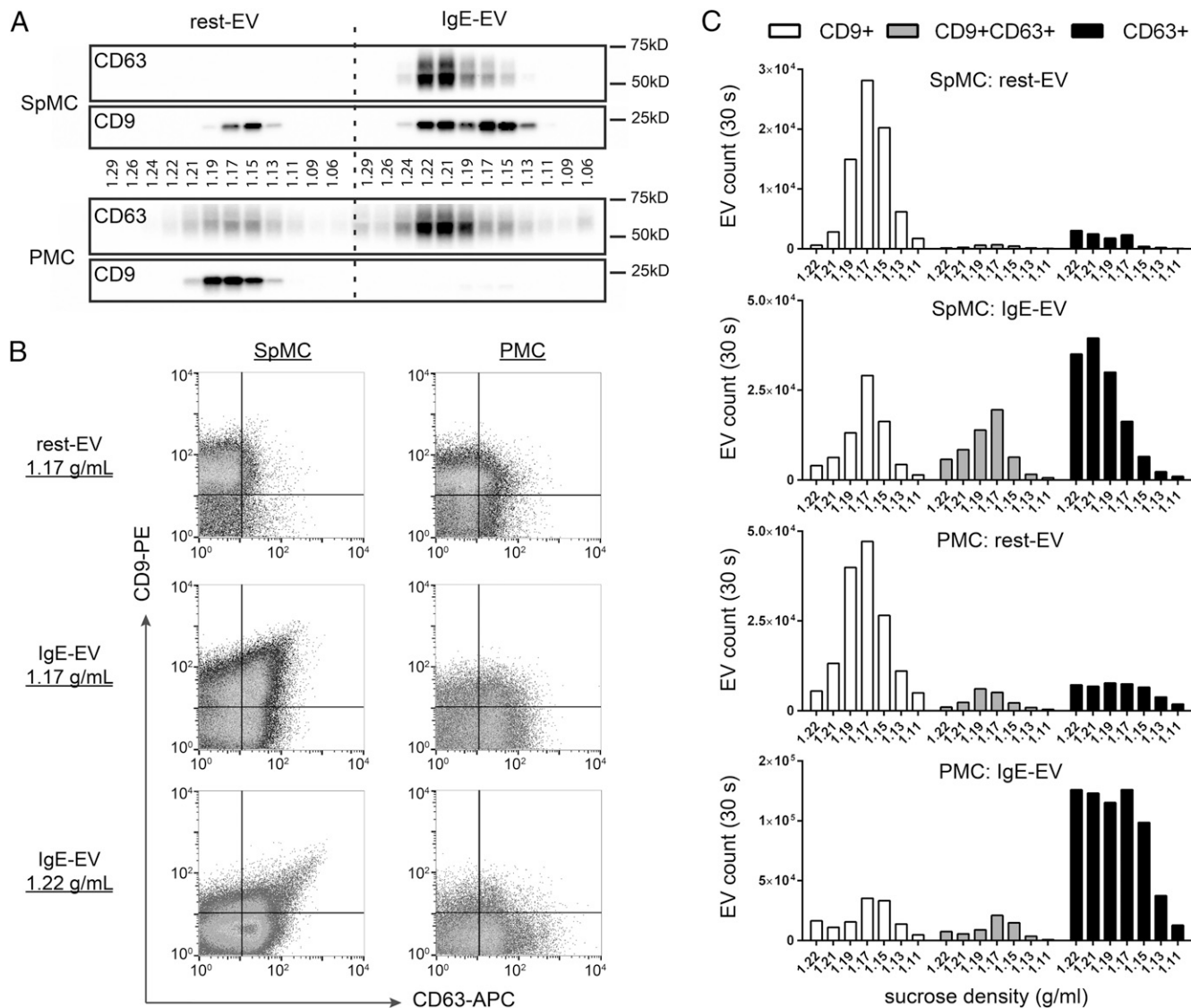

FIGURE 2. CD9 and CD63 contents of EV derived from unstimulated or degranulated MC are markedly different. EV were isolated from supernatants and floated into sucrose density gradients. (**A**) Western blot analysis of SpMC-derived EV (upper panel) and PMC-derived EV (lower panel) from equal cell numbers were isolated from separate sucrose fractions and run on a 10% gel. rest-EV and IgE-EV released from equal cell numbers were analyzed for their CD9 and CD63 content for each polyvinylidene difluoride membrane. The dashed vertical line indicates the separation of rest-EV and IgE-EV fractions. (**B**) EV were stained with PKH67, anti-CD9 PE, and anti-CD63 allophycocyanin prior to flotation for high-resolution flow cytometric analysis. Representative dot plots of CD9/CD63 detection on single SpMC-derived EV and PMC-derived EV that had clearly distinct buoyant densities in sucrose gradients, 1.17 g/ml and 1.22 g/ml (lines indicate gating strategy by which <2% background events are observed when using isotype control Ab). (**C**) Number of EV recorded in 30 s that are single positive or double positive for CD9 and CD63. Results are representative of at least two independent experiments.

release of β-hexosaminidase (Fig. 3A, 3B), degranulating strength, and type of stimulus (Fig. 3C, 3D). Corresponding with the fact that SpMC represent the MMC phenotype, degranulation could not be triggered with SP and c48/80, and EV release was not increased under these conditions. Independently of the strength and type of stimulation, MC released the same EV population upon degranulation (i.e., primarily CD63 single positive, but also some CD9 single- and CD9/CD63 double-positive EV derived from SpMC (Fig. 3E, 3F). Note that these analyses were performed on EV floated into iodixanol gradients, which resulted in the accumulation of most EV in a small volume (less fractions compared with sucrose gradients). Together, these findings indicate that the rate of EV release is tightly correlated with degranulation and is independent on the type of stimulus triggering degranulation.

Increased EV release is not a general feature of MC activation

Activation of MC via alternative mechanisms, such as TLR4-mediated activation by LPS, does not result in degranulation (Fig. 4A), but it readily leads to cytokine production and release within hours (e.g., IL-6) (Fig. 4B). To investigate the effect of this type of MC activation on EV release, EV were analyzed after LPS activation and compared with unstimulated conditions. In contrast to IgE-mediated activation, activation with LPS for 1.5 h did not result in enhanced EV release (Fig. 4C). Under these conditions,

EV numbers were comparable to those found in supernatants from unstimulated controls after 1.5 h of culture (data not shown). Also, overnight activation of MC with LPS did not significantly change the total numbers of released EV compared with rest-EV (SpMC: $n = 5$, $p = 0.43$; PMC: $n = 3$, $p = 0.59$; Fig. 4C) or influence the CD9/CD63 content of EV (i.e., most EV were CD9 single positive comparable to rest-EV; SpMC: $n = 5$, percentage of CD9$^+$ $p = 0.82$, percentage of CD9$^+$CD63$^+$ $p = 0.12$, percentage of CD63$^+$ $p = 0.39$; PMC: $n = 3$, percentage of CD9$^+$ $p = 0.09$, percentage of CD9$^+$CD63$^+$ $p = 0.55$, percentage of CD63$^+$ $p = 0.17$; Fig. 4D). These data show that the release of high EV numbers is not a general result of MC activation but is correlated with the degree of degranulation.

EV derived from unstimulated and degranulated MC differ in lipid composition

Based on our finding that rest-EV and IgE-EV differ in buoyant density, size, and CD9/CD63 content, we next investigated whether these different MC-EV subsets also displayed differences in phospholipid composition. The presence of specific lipid species on distinct EV subsets might be indicative of their subcellular origin (50–53) or their functional properties (54). Principal component analysis using all individual phospholipids that were identified (ceramides were excluded because their elution from the column
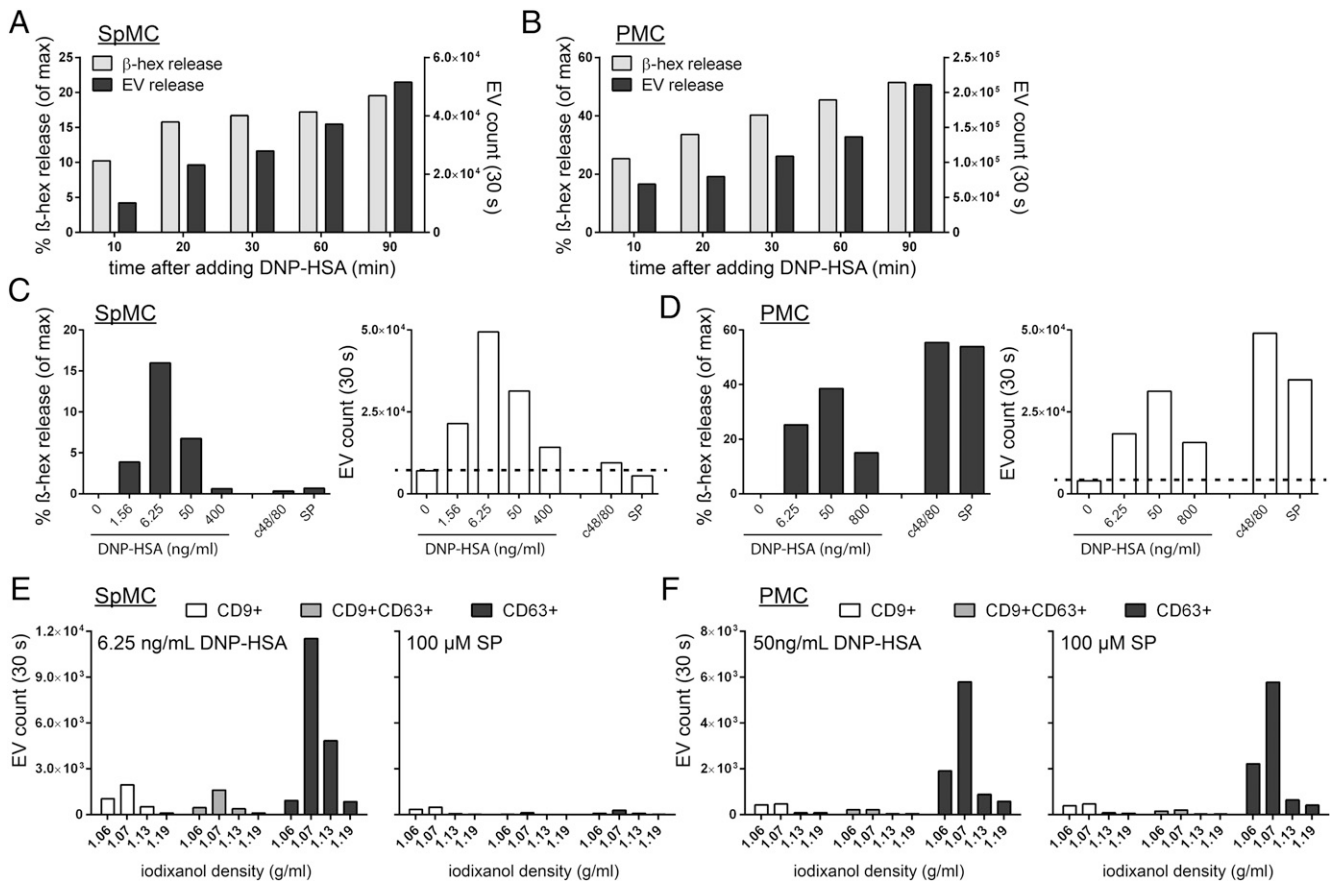

FIGURE 3. Increased EV release correlates with MC degranulation. DNP-IgE–primed SpMC (**A**) and PMC (**B**) were activated with an optimal concentration of DNP-HSA, and culture supernatants were collected at multiple times. EV were isolated and labeled with CFSE ($n = 1$). DNP-IgE–primed SpMC (**C**) and PMC (**D**) were activated with different concentrations of DNP-HSA, 10 μg/ml c48/80, or 100 μM SP, and culture supernatants were collected after 1.5 h. EV were isolated and labeled with CFSE, anti-CD9 allophycocyanin, and anti-CD63 PE. (A–D) After labeling, EV were floated into iodixanol gradients and analyzed by high-resolution flow cytometry. The total number of events indicated is the sum of EV counts recorded in 30 s in density fractions from 1.05 to 1.19 g/ml. The extent of degranulation was determined by measuring β-hexosaminidase release. The dashed lines in (C) and (D) indicate the event counts of EV released from unstimulated cells. (**E** and **F**) Number of EV that are single positive or double positive for CD9 and CD63 per density fraction, as recorded in the 30-s measurements indicated in (C) and (D). Representative samples are shown to illustrate EV release during optimal and supraoptimal IgE-mediated degranulation and after addition of SP. Data in (C)–(F) are representative of three independent experiments.
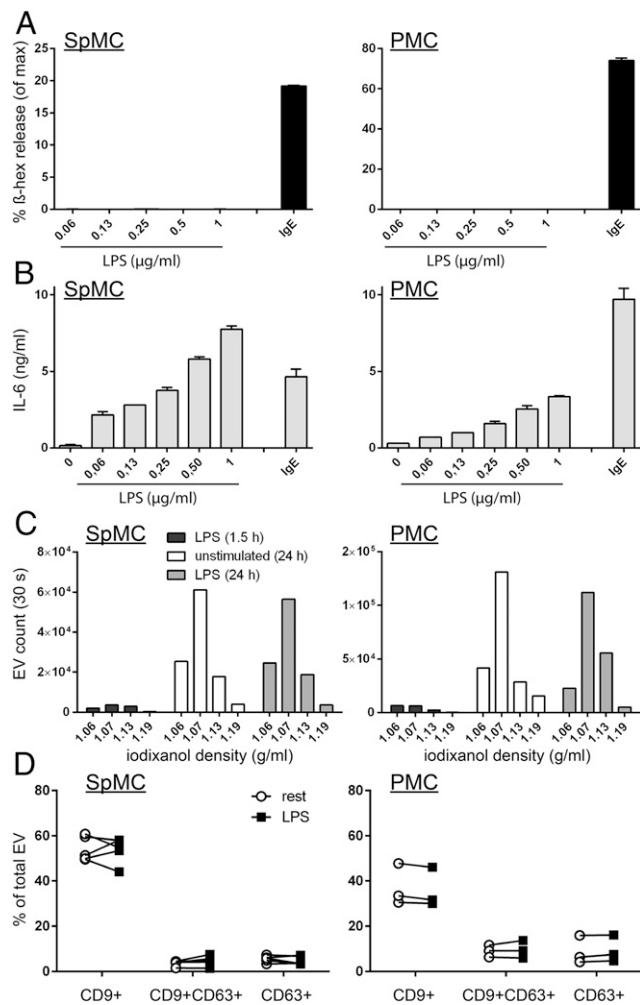
FIGURE 4. LPS-mediated MC activation does not induce enhanced release of EV. (**A**) β-hexosaminidase release was measured 1.5 h after incubation with different concentrations of LPS or after IgE-mediated degranulation using optimal conditions. (**B**) Using similar conditions as in (A), IL-6 release was measured after a 24-h culture. Results are representative of two independent experiments. (**C**) MC were stimulated for 1.5 or 24 h with LPS (1 μg/ml) or were cultured unstimulated for 24 h, followed by EV isolation from culture supernatants. EV were labeled with CFSE, anti-CD9 PE, and anti-CD63 allophycocyanin, floated into iodixanol density gradients, and quantified using high-resolution flow cytometry. Data shown are the number of events recorded in 30 s. (**D**) During the same analysis in multiple experiments, the number of single- or double-positive EV for CD9 and CD63 was recorded and is shown as a percentage of total EV. Paired *t* tests were performed to analyze changes in CD9 and CD63 content between EV released by unstimulated or LPS-activated MC (connected by lines for independent experiments). Results are representative of five (SpMC) and three (PMC) independent experiments.

was considered to be too close to the solvent front) showed, despite interexperimental variance, clear differences between rest-EV and IgE-EV (Fig. 5A). Interestingly, this difference was largely independent of the producing MC phenotype. Therefore, data from both phenotypes were combined to further analyze major differences between rest-EV and IgE-EV. Comparison of the phospholipid classes showed a particular enrichment of phosphatidylinositol in IgE-EV ($p < 0.001$) and phosphatidic acid in rest-EV ($p < 0.001$) (Fig. 5B). Analysis of individual phospholipid species revealed more pronounced differences between the EV subsets. In total, 46 of 154 identified species showed a significantly different distribution between rest-EV and

IgE-EV (Supplemental Table I), including differences in certain bis(monoacylglycero)phosphate (BMP; also incorrectly termed lysobisphosphatidic acid) (6 of 27), phosphatidylcholine (13 of
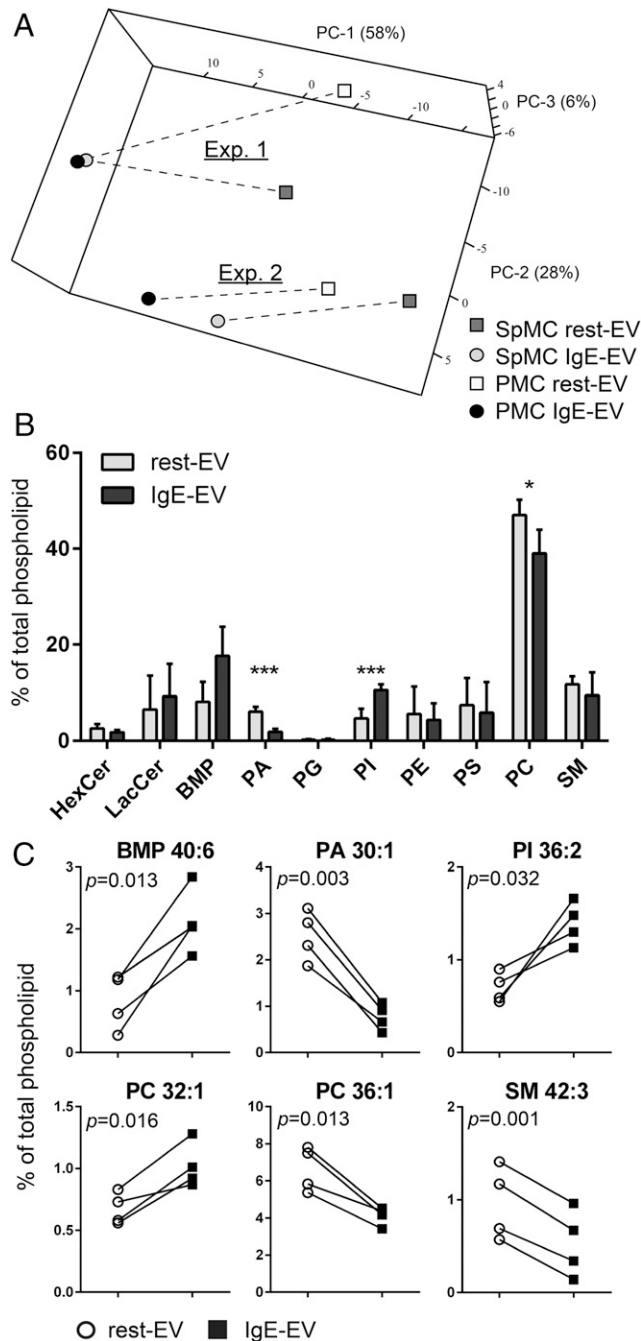
FIGURE 5. rest-EV and IgE-EV show a distinct phospholipid composition. EV were isolated from culture supernatants and floated into iodixanol density gradients. After pelleting EV from fractions with a density between 1.05 and 1.13 g/ml, phospholipids were extracted and analyzed by LC-MS. (**A**) Principal component analysis of combined data from two independent experiments. (**B**) Relative abundance of the main phospholipid classes in rest-EV and SpMC-derived EV. (**C**) Examples of abundant phospholipid species showing distinct contributions to EV composition of both EV subsets. For (B) and (C), rest-EV and IgE-EV data were combined, independent of MC phenotype. *$p < 0.05$, ***$p < 0.001$, paired *t* test, rest-EV versus IgE-EV. HexCer, monohexosylceramides; LacCer, lactosylceramide; PA, phosphatidic acid; PC, phosphatidylcholine; PE, phosphatidylethanolamine; PG, phosphatidylglycerol; PI, phosphatidylinositol; PS, phosphatidylserine; SM, sphingomyelin.

44), lactosylceramide (2 of 15), and sphingomyelin (2 of 12) species. Examples of abundant phospholipids that showed a significantly distinctive contribution to rest-EV and IgE-EV composition are shown in Fig. 5C. The presence of saturated phospholipids did not differ between EV subsets and was relatively low (ranging from 24% to 91% per subclass). A similar lipid analysis was performed on $100,000 \times g$ pelleted material derived from culture medium containing 10 or 1% EV-depleted FCS to exclude that observed differences were a result of differences in culture medium. No significant amounts of phospholipids were identified in these analyses (data not shown). In conclusion, IgE-EV membranes are enriched for phosphatidylinositol and certain BMP species, whereas rest-EV contain substantially higher levels of phosphatidic acid. Interestingly, because BMP is associated selectively with late endosomes and lysosomes (51, 53, 55), and CD63 has been associated with BMP-rich internal membranes of late endosomes (56), this suggests that IgE-EV originate from the endosomal/lysosomal pathway.

IgE-EV released by PMC contain MC-specific proteases

Our data indicate that the release of high numbers of EV is associated with MC degranulation and that the tetraspanin and lipid content of these EV is indicative of an endosomal/lysosomal origin. Next, proteomic analysis of IgE-EV was performed to explore whether these EV contain proteins associated with MC secretory granules/lysosomes. The analysis was performed on PMC IgE-EV because PMC highly expressed known CTMC-associated proteases (Supplemental Fig. 1D). In addition to common EV-associated proteins (e.g., Rab proteins, HSP70, and HSP90) and cytoskeletal proteins β-actin and tubulin, MC-related proteins (e.g., CD117 and Fc receptor γ-chain) were identified (Table I, Supplemental Table II). Western blot analyses for HSP70, HSP90, CD117, and the γ-chain confirmed their relative abundance in IgE-EV (Fig. 6A). Remarkably, the MC-specific proteases CPA3, mMCP4, mMCP5, and mMCP6 were detected in PMC IgE-EV by proteomics (Table I). These proteases are usually considered true soluble mediators released after degranulation. In contrast, β-hexosaminidase or the PMC granule-associated proteoglycan heparin was not identified. Because CPA3 was the most abundant protease detected, its association with EV was verified by Western blotting. A clear band was detected in IgE-EV at ~36 kDa, which corresponds to the mature and active form of CPA3 (57) (Fig. 6A). The catalytic

activity of EV-associated CPA3 was assessed by measuring cleavage of the CPA3-specific substrate *N*-(4-methoxyphenylazoformyl)-L-phenylalanine (44). The specificity of this assay was confirmed using lysates of cells containing high (PMC), low/moderate (SpMC), or no (bone marrow–derived dendritic cells [BMDC]) CPA3 activity (Fig. 6B). To address whether the catalytic activity of CPA3 present in supernatant of degranulated PMC could be ascribed to EV-associated CPA3, PMC culture supernatant was subjected to different centrifugation steps prior to the hydrolysis assay. Although centrifugation at $500 \times g$ did not affect CPA3 activity, substrate hydrolysis was reduced significantly in the supernatant after the $10,000 \times g$ pelleting step, as expected, because the depleted pellets contain granule remnants and, thus, large quantities of proteoglycan-associated proteases. The subsequent $100,000 \times g$ pelleting step, required for EV isolation, significantly reduced substrate hydrolysis even further (Fig. 6C), suggesting that active CPA3 is also associated with EV. This loss of enzyme activity by ultracentrifugation was not observed for β-hexosaminidase (Supplemental Fig. 2D). To further investigate the possible association of CPA3 and IgE-EV, PMC and SpMC IgE-EV were purified using iodixanol density gradients. The observed CPA3 activity, especially in PMC IgE-EV, indicated that CPA3 is indeed EV associated (Fig. 6D). By analyzing decline rates of substrate degradation of multiple sample dilutions of both culture supernatants and EV isolates in two independent experiments, it was calculated that, on average, 10% (9.1 and 11.0%) of all released CPA3 is associated with IgE-EV that were pelleted at $100,000 \times g$. Finally, to confirm that CPA3 floated in association with EV and was not present throughout the gradient, PMC-derived IgE-EV from individual density fractions were pelleted and analyzed. CPA3 activity was primarily found at a density of 1.07 g/ml, in line with the density at which the majority of EV floated (Fig. 6E). Substantial CPA3 activity also was observed in the EV-containing density fraction of 1.13 g/ml, but not at densities < 1.07 g/ml or densities > 1.13 g/ml, indicating that CPA3 was not diffusely present in the gradient. Together, these data show that active CPA3 released from degranulated MC can be released in an EV-associated form.

Discussion

Although the involvement of MC in immune disorders and immune modulation is increasingly appreciated, their mode of action is

Table I. Selection of proteins identified by proteomic analysis of IgE-EV released by PMC

| Description	Protein Name, Alternative Names	Coverage (%)	No. of Peptides	No. of PSM
CBPA3	MC carboxypeptidase A, CPA3	46.04	22	86
CMA1	MC chymase 1, mMCP5	53.44	17	55
AMPN	Aminopeptidase N, AP-N, CD13, p161	16.87	14	22
ACTB	Actin, cytoplasmic 1, β-actin	35.73	14	21
MCPT4	Chymase, mMCP4	29.67	5	12
ACTBL	β-actin–like protein 2, κ-actin	13.03	4	5
HSP7C	Heat shock cognate 71 kDa protein, hsc70	9.91	5	5
KIT	c-KIT, CD117, mast/stem cell growth factor receptor	4.80	5	5
TRYB2	Tryptase β-2, tryptase-2, mMCP-6	14.86	3	4
ILRL1	IL-1R–like 1, protein ST2	6.35	3	3
PAFA	Platelet-activating factor acetylhydrolase	5.68	2	2
TBA1C	Tubulin α-1C, α tubulin 6	2.23	1	1
HS90B	HSP90-β, HSP84, TSTA	1.66	1	1
CD63	CD63	4.20	1	1
RAB35	Ras-related protein, Rab35	5.47	1	1
LAMP2	Lysosome-associated membrane (glyco)protein 2, CD107b	1.93	1	1
FCERG	Fc receptor γ-chain, Fc-ε RI-γ	17.44	1	1
RAB7A	Ras-related protein, Rab7a	5.31	1	1

PSM, peptide-spectrum match.
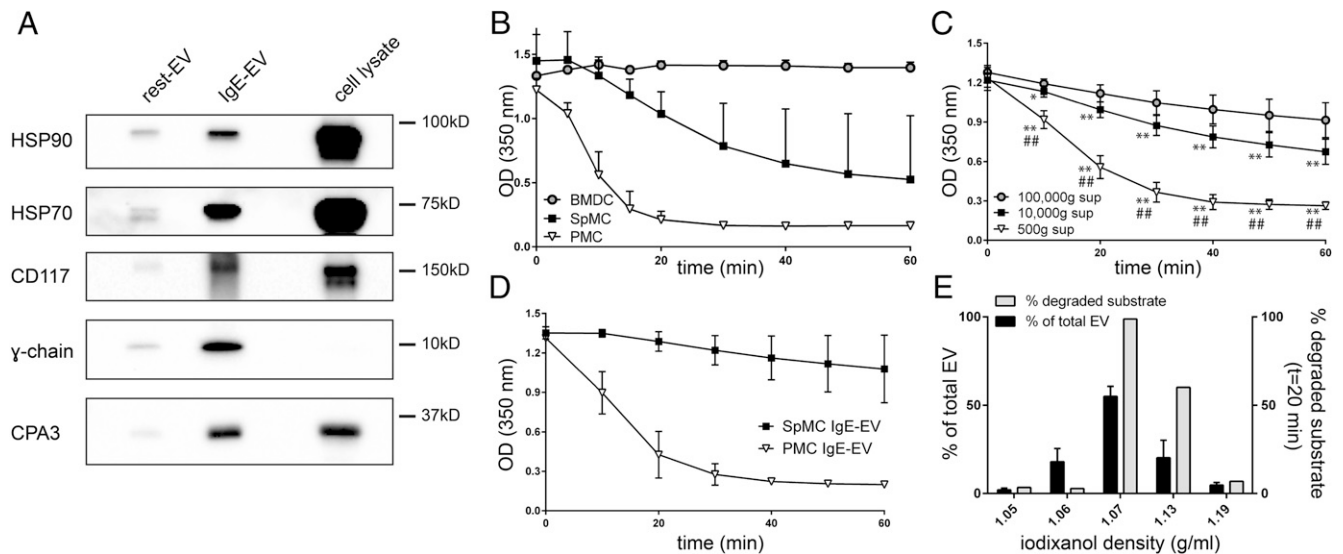
FIGURE 6. PMC-derived EV contain common EV-associated and MC-specific proteins. (**A**) Western blot analysis of rest-EV and IgE-EV derived from equal numbers of PMC. Isolated EV were floated into iodixanol density gradients. EV floating at densities between 1.05 and 1.13 g/ml were pooled, pelleted, resuspended in Laemmli buffer, and loaded onto a 10% gel. PMC lysate (80,000 cells) was included as a positive control. Results are representative of at least two independent experiments. (**B**) Cell lysates from different cell types were tested to assess the specificity of the CPA3 activity assay. SpMC, PMC, and BMDC lysates were prepared in PBS/2M NaCl/0.5% TX-100, and volumes equal to $n = 100,000$ cells were used to assess CPA3-specific substrate degradation for 60 min (absorbance at OD_{350}). Error bars indicate SDs (PMC, $n = 4$) or range (BMDC and SpMC, $n = 2$). (**C**) Culture supernatants collected after IgE-mediated PMC degranulation were centrifuged at $500 \times g$, $10,000 \times g$, and $100,000 \times g$ and analyzed for CPA3 activity. Error bars indicate SDs (seven independent experiments). Differences in substrate degradation were analyzed using a two-way ANOVA followed by a Tukey multiple-comparison test. (**D**) After IgE-mediated degranulation, IgE-EV from PMC and SpMC were isolated from the culture supernatant and floated into iodixanol density gradients. EV floating at densities between 1.05 and 1.13 g/ml were pooled, pelleted, and analyzed for CPA3 activity. Error bars indicate SDs (PMC IgE-EV, $n = 3$) or range (SpMC IgE-EV, $n = 2$). (**E**) IgE-EV from PMC floating at densities 1.05, 1.06, 1.07, 1.13, and 1.19 g/ml were collected separately, pelleted, and analyzed for CPA3 activity. The percentage of degraded substrate 20 min after addition of EV to the substrate was compared with the distribution of EV in iodixanol gradients (average of nine independent EV counts). In all CPA3 assays, the absorbance at OD_{350} was monitored for 60 min at 37°C. Results are representative of three independent experiments. $*p < 0.05$, $**p < 0.0001$, versus $100,000 \times g$ supernatant; $^{\#\#}p < 0.0001$, versus $10,000 \times g$ supernatant.

often poorly understood. An appealing question is whether MC-EV contribute to this function, because many EV types are associated with immune-modulation (15, 16). Compared with soluble mediators, EV-mediated transfer of functional components has several advantages. In addition to the protection of cargo from degradation, the combination of different functional molecules into a single EV and the (sub)cellular targeting can lead to different cellular responses in target cells compared with responses induced by the individual components (58). Furthermore, membrane-associated proteins can induce more potent responses than soluble proteins, as was shown for EV-associated HSP70 (59).

In this study, we used two functionally different MC phenotypes to analyze the release, molecular contents, and proteolytic capacity of MC-EV to gain more insight into their function in immune responses. We showed that SpMC and PMC release EV in resting conditions and can be stimulated to release high quantities of an EV subset that substantially differs in buoyant density, size, and lipid composition upon degranulation. In this latter condition, we observed comparable release rates of these IgE-EV and soluble preformed mediators (detectable within minutes) (11). This rapid release was not a general consequence of MC activation because neither short nor prolonged TLR4-mediated stimulation, without degranulation, enhanced EV release.

In addition to the release of submicron EV, degranulation of MC results in the release of ~1 μm–sized heparin-based particles that traffic to draining lymph nodes where they induce lymph node remodeling (60). Possibly, the MC-EV released after degranulation traffic to similar distant sites where they exert unknown

functions. Previously, it was suggested that dendritic cells are a possible target for MC-EV (24). However, whether the observed effects were truly EV mediated remain unclear as a result of limitations in the EV-isolation protocols used. Protein aggregates or larger particles (like the heparin-based particles) could have been responsible for the observed effects, because a preclearing $10,000 \times g$ pelleting step and separation of EV from protein aggregates by density gradient separation were omitted. We are analyzing immune-modulatory effects of the different subsets of purified MC-EV using the optimized EV isolation and release protocols.

Although it is most likely that the EV population released upon MC degranulation derived from MC secretory granules, we cannot fully exclude that EV release and β-hexosaminidase release are coincident events that are independent, but both rely on increased intracellular calcium concentrations (61–63). However, because no discriminatory markers are available to distinguish EV budding from the plasma membrane (often termed microvesicles) from EV that originate from the endosomal route (often termed exosomes), this possibility cannot be addressed (31). Previously, electron microscopy studies showed the presence of vesicles in different types of MC granules (22). The majority of these vesicles ranged from 60 to 80 nm in diameter, comparable to the size of IgE-EV characterized in our study, and were released upon degranulation. Interestingly, similar findings were described for cytotoxic T cells that, like MC, contain secretory granules/lysosomes (64, 65). This colocalization of vesicles and electron-dense cores filled with preformed compounds (22) [including proteases and lysosomal enzymes (1)] supports the correlation between IgE-EV and

β-hexosaminidase release observed in this study. The high CD63 content of IgE-EV further supports an endocytic origin of the vesicles, because CD63, in contrast to CD9, is abundant in the limiting membrane of MC granules (66). Another granule-related transmembrane protein, CD107b (LAMP-2), was detected in IgE-EV by proteomics and was found earlier to localize to small intraluminal vesicles (22). Moreover, IgE-EV contained Rab7, a late endosome-associated Rab involved in secretion of exosomes containing syntenin-1 (also identified in IgE-EV), and Rab35, another Rab family member implicated in intracellular vesicle trafficking and exosome release (67, 68). Also, the phospholipid composition of IgE-EV is indicative of a secretory granule/lysosomal origin. Although BMP was only weakly detected or was not detected in EV preparations in previous studies (26, 69), it was a relatively abundant phospholipid in the MC-EV analyzed in this study, especially IgE-EV. BMP is selectively and abundantly present in the inner membranes of late endosomes, in particular lysosomes (51, 53, 55), and it is involved in trafficking of proteins and lipids (53, 70), vesicle formation, and vesicle stabilization (52, 71). BMP also facilitates attachment of cationic enzymes because of its negative charge (55) and, thus, can provide a mechanism for the incorporation of the identified proteases into IgE-EV. Moreover, CD63 was found within a complex network of BMP-rich internal membranes of late endosomes of endothelial cells (56), which is in line with the high CD63 content of IgE-EV. In addition to these differences for BMP, the multiple differences in the phospholipid content of rest-EV versus IgE-EV, including the notable disparate enrichment in phosphatidylinositol and phosphatidic acid, might be indicative of differences in their biogenesis.

The proteomics analysis of PMC IgE-EV unveiled the remarkable presence of many MC-specific proteases. No previous study examined their true presence in EV or EV-associated enzyme activity. An online search of the Vesiclepedia database (72) indicated that CPA3 and mMCP5 were identified in $100,000 \times g$ pellets in one study (29) investigating the murine MC line MC/9. We provide strong evidence that MC proteases are indeed associated with EV. Importantly, as shown for CPA3, ≥10% of the released protein is EV associated and biologically active. These findings shed new light on the current dogma that these enzymes are only released as true soluble mediators that can be retained in proteoglycan matrices in close proximity to the releasing MC (73). Association of the enzymes with EV might be a mechanism to transfer an effective combination of enzymes to specific distant target sites where they could be involved in multiple and diverse processes, such as proteolytic processing or degradation of cytokines and chemokines, degradation of endothelin-1 or toxins, generation of angiotensin II, or activation of proteinase-activated receptor 2 (reviewed in Refs. 38, 39, 74, 75). Similar to rodents, different human MC phenotypes exist that can express a variable combination of tryptase, chymase, and CPA3. Human MC-specific proteases show substantial homologies with the EV-associated proteases found in this study (38, 76), suggesting that these might also be contained in EV in humans.

In conclusion, upon MC degranulation, large quantities of CD63-positive EV are released comprising (MC-specific) protease activities. Because MC are immune sentinel cells that play a role in many (patho)physiological immune processes, this study unveils MC-EV as potentially important vehicles for immune regulation.

Acknowledgments

Disclosures

The authors have no financial conflicts of interest.

References

1. Moon, T. C., C. D. St Laurent, K. E. Morris, C. Marcet, T. Yoshimura, Y. Sekar, and A. D. Befus. 2010. Advances in mast cell biology: new understanding of heterogeneity and function. *Mucosal Immunol.* 3: 111–128.
2. da Silva, E. Z. M., M. C. Jamur, and C. Oliver. 2014. Mast cell function: a new vision of an old cell. *J. Histochem. Cytochem.* 62: 698–738.
3. Galli, S. J., M. Grimbaldeston, and M. Tsai. 2008. Immunomodulatory mast cells: negative, as well as positive, regulators of immunity. *Nat. Rev. Immunol.* 8: 478–486.
4. Galli, S. J., and M. Tsai. 2010. Mast cells in allergy and infection: versatile effector and regulatory cells in innate and adaptive immunity. *Eur. J. Immunol.* 40: 1843–1851.
5. Abraham, S. N., and A. L. St John. 2010. Mast cell-orchestrated immunity to pathogens. *Nat. Rev. Immunol.* 10: 440–452.
6. Carroll-Portillo, A., J. L. Cannon, J. te Riet, A. Holmes, Y. Kawakami, T. Kawakami, A. Cambi, and D. S. Lidke. 2015. Mast cells and dendritic cells form synapses that facilitate antigen transfer for T cell activation. *J. Cell Biol.* 210: 851–864.
7. Nakae, S., H. Suto, M. Iikura, M. Kakurai, J. D. Sedgwick, M. Tsai, and S. J. Galli. 2006. Mast cells enhance T cell activation: importance of mast cell costimulatory molecules and secreted TNF. *J. Immunol.* 176: 2238–2248.
8. Shelburne, C. P., H. Nakano, A. L. St John, C. Chan, J. B. McLachlan, M. D. Gunn, H. F. Staats, and S. N. Abraham. 2009. Mast cells augment adaptive immunity by orchestrating dendritic cell trafficking through infected tissues. *Cell Host Microbe* 6: 331–342.
9. Rodrigues, C. P., A. C. Ferreira, M. P. Pinho, C. J. de Moraes, P. C. Bergami-Santos, and J. A. Barbuto. 2016. Tolerogenic IDO(+) dendritic cells are induced by PD-1-expressing mast cells. *Front. Immunol.* 7: 9 doi:10.3389/fimmu.2016.00009.
10. Suurmond, J., J. van Heemst, J. van Heiningen, A. L. Dorjée, M. W. Schilham, F. B. van der Beek, T. W. Huizinga, A. J. Schuerwegh, and R. E. Toes. 2013. Communication between human mast cells and CD4(+) T cells through antigen-dependent interactions. *Eur. J. Immunol.* 43: 1758–1768.
11. Galli, S. J., J. Kalesnikoff, M. A. Grimbaldeston, A. M. Piliponsky, C. M. Williams, and M. Tsai. 2005. Mast cells as "tunable" effector and immunoregulatory cells: recent advances. *Annu. Rev. Immunol.* 23: 749–786.
12. Blank, U. 2011. The mechanisms of exocytosis in mast cells. *Adv. Exp. Med. Biol.* 716: 107–122.
13. Matsushima, H., N. Yamada, H. Matsue, and S. Shimada. 2004. TLR3-, TLR7-, and TLR9-mediated production of proinflammatory cytokines and chemokines from murine connective tissue type skin-derived mast cells but not from bone marrow-derived mast cells. *J. Immunol.* 173: 531–541.
14. Varadaradjalou, S., F. Féger, N. Thieblemont, N. B. Hamouda, J.-M. Pleau, M. Dy, and M. Arock. 2003. Toll-like receptor 2 (TLR2) and TLR4 differentially activate human mast cells. *Eur. J. Immunol.* 33: 899–906.
15. Robbins, P. D., and A. E. Morelli. 2014. Regulation of immune responses by extracellular vesicles. *Nat. Rev. Immunol.* 14: 195–208.
16. Nolte-'t Hoen, E. N., and M. H. Wauben. 2012. Immune cell-derived vesicles: modulators and mediators of inflammation. *Curr. Pharm. Des.* 18: 2357–2368.
17. Tickner, J. A., A. J. Urquhart, S. A. Stephenson, D. J. Richard, and K. J. O'Byrne. 2014. Functions and therapeutic roles of exosomes in cancer. *Front. Oncol.* 4: 127 doi:10.3389/fonc.2014.00127.
18. Loyer, X., A.-C. Vion, A. Tedgui, and C. M. Boulanger. 2014. Microvesicles as cell-cell messengers in cardiovascular diseases. *Circ. Res.* 114: 345–353.
19. Théry, C., M. Ostrowski, and E. Segura. 2009. Membrane vesicles as conveyors of immune responses. *Nat. Rev. Immunol.* 9: 581–593.
20. Nolte-'t Hoen, E. N., E. J. van der Vlist, M. de Boer-Brouwer, G. J. Arkesteijn, W. Stoorvogel, and M. H. Wauben. 2013. Dynamics of dendritic cell-derived vesicles: high-resolution flow cytometric analysis of extracellular vesicle quantity and quality. *J. Leukoc. Biol.* 93: 395–402.
21. Gould, S. J., and G. Raposo. 2013. As we wait: coping with an imperfect nomenclature for extracellular vesicles. *J. Extracell. Vesicles* 2: 20389 doi:10.3402/jev.v2i0.20389.
22. Raposo, G., D. Tenza, S. Mecheri, R. Peronet, C. Bonnerot, and C. Desaymard. 1997. Accumulation of major histocompatibility complex class II molecules in mast cell secretory granules and their release upon degranulation. *Mol. Biol. Cell* 8: 2631–2645.
23. Skokos, D., S. Le Panse, I. Villa, J.-C. Rousselle, R. Peronet, B. David, A. Namane, and S. Mécheri. 2001. Mast cell-dependent B and T lymphocyte activation is mediated by the secretion of immunologically active exosomes. *J. Immunol.* 166: 868–876.
24. Skokos, D., H. G. Botros, C. Demeure, J. Morin, R. Peronet, G. Birkenmeier, S. Boudaly, and S. Mécheri. 2003. Mast cell-derived exosomes induce phenotypic and functional maturation of dendritic cells and elicit specific immune responses in vivo. *J. Immunol.* 170: 3037–3045.
25. Subra, C., D. Grand, K. Laulagnier, A. Stella, G. Lambeau, M. Paillasse, P. De Medina, B. Monsarrat, B. Perret, S. Silvente-Poirot, et al. 2010. Exosomes account for vesicle-mediated transcellular transport of activatable phospholipases and prostaglandins. *J. Lipid Res.* 51: 2105–2120.
26. Laulagnier, K., C. Motta, S. Hamdi, S. Roy, F. Fauvelle, J.-F. Pageaux, T. Kobayashi, J.-P. Salles, B. Perret, C. Bonnerot, and M. Record. 2004. Mast cell- and dendritic cell-derived exosomes display a specific lipid composition and an unusual membrane organization. *Biochem. J.* 380: 161–171.

27. Carroll-Portillo, A., Z. Surviladze, A. Cambi, D. S. Lidke, and B. S. Wilson. 2012. Mast cell synapses and exosomes: membrane contacts for information exchange. *Front. Immunol.* 3: 46 doi:10.3389/fimmu.2012.00046.

28. Eldh, M., K. Ekström, H. Valadi, M. Sjöstrand, B. Olsson, M. Jernås, and J. Lötvall. 2010. Exosomes communicate protective messages during oxidative stress; possible role of exosomal shuttle RNA. *PLoS One* 5: e15353.

29. Valadi, H., K. Ekström, A. Bossios, M. Sjöstrand, J. J. Lee, and J. O. Lötvall. 2007. Exosome-mediated transfer of mRNAs and microRNAs is a novel mechanism of genetic exchange between cells. *Nat. Cell Biol.* 9: 654–659.

30. Witwer, K. W., E. I. Buzás, L. T. Bemis, A. Bora, C. Lässer, J. Lötvall, E. N. Nolte-'t Hoen, M. G. Piper, S. Sivaraman, J. Skog, et al. 2013. Standardization of sample collection, isolation and analysis methods in extracellular vesicle research. *J. Extracell. Vesicles* 2: 20360 doi:10.3402/jev.v2i0.20360.

31. Lötvall, J., A. F. Hill, F. Hochberg, E. I. Buzás, D. Di Vizio, C. Gardiner, Y. S. Gho, I. V Kurochkin, S. Mathivanan, P. Quesenberry, et al. 2014. Minimal experimental requirements for definition of extracellular vesicles and their functions: a position statement from the International Society for Extracellular Vesicles. *J. Extracell. Vesicles* 3: 26913 doi:10.3402/jev.v3.26913.

32. Gurish, M. F., and K. F. Austen. 2012. Developmental origin and functional specialization of mast cell subsets. *Immunity* 37: 25–33.

33. van der Vlist, E. J., E. N. Nolte-'t Hoen, W. Stoorvogel, G. J. Arkesteijn, and M. H. Wauben. 2012. Fluorescent labeling of nano-sized vesicles released by cells and subsequent quantitative and qualitative analysis by high-resolution flow cytometry. *Nat. Protoc.* 7: 1311–1326.

34. Nolte-'t Hoen, E. N., E. J. van der Vlist, M. Aalberts, H. C. Mertens, B. J. Bosch, W. Bartelink, E. Mastrobattista, E. V. van Gaal, W. Stoorvogel, G. J. Arkesteijn, and M. H. Wauben. 2012. Quantitative and qualitative flow cytometric analysis of nanosized cell-derived membrane vesicles. *Nanomedicine* 8: 712–720.

35. Malbec, O., K. Roget, C. Schiffer, B. Iannascoli, A. R. Dumas, M. Arock, and M. Daëron. 2007. Peritoneal cell-derived mast cells: an in vitro model of mature serosal-type mouse mast cells. *J. Immunol.* 178: 6465–6475.

36. Krüger, P. G., D. Lagunoff, and H. Wan. 1980. Isolation of rat mast cell granules with intact membranes. *Exp. Cell Res.* 129: 83–93.

37. Lindstedt, K. A., and P. T. Kovanen. 2006. Isolation of mast cell granules. *Curr. Protoc. Cell Biol.* Chapter 3: Unit 3.16.

38. Pejler, G., E. Rönnberg, I. Waern, and S. Wernersson. 2010. Mast cell proteases: multifaceted regulators of inflammatory disease. *Blood* 115: 4981–4990.

39. Wernersson, S., and G. Pejler. 2014. Mast cell secretory granules: armed for battle. *Nat. Rev. Immunol.* 14: 478–494.

40. Groot Kormelink, T., G. J. Arkesteijn, F. A. Nauwelaers, G. van den Engh, E. N. Nolte-'t Hoen, and M. H. Wauben. 2016. Prerequisites for the analysis and sorting of extracellular vesicle subpopulations by high-resolution flow cytometry. *Cytometry A* 89: 135–147.

41. Bligh, E. G., and W. J. Dyer. 1959. A rapid method of total lipid extraction and purification. *Can. J. Biochem. Physiol.* 37: 911–917.

42. Tautenhahn, R., C. Böttcher, and S. Neumann. 2008. Highly sensitive feature detection for high resolution LC/MS. *BMC Bioinformatics* 9: 504 doi:10.1186/1471-2105-9-504.

43. Patyshakuliyeva, A., H. Post, M. Zhou, E. Jurak, A. J. Heck, K. S. Hildén, M. A. Kabel, M. R. Mäkelä, M. A. Altelaar, and R. P. de Vries. 2015. Uncovering the abilities of *Agaricus bisporus* to degrade plant biomass throughout its life cycle. *Environ. Microbiol.* 17: 3098–3109.

44. Mock, W. L., Y. Liu, and D. J. Stanford. 1996. Arazoformyl peptide surrogates as spectrophotometric kinetic assay substrates for carboxypeptidase A. *Anal. Biochem.* 239: 218–222.

45. Feyerabend, T. B., H. Hausser, A. Tietz, C. Blum, L. Hellman, A. H. Straus, H. K. Takahashi, E. S. Morgan, A. M. Dvorak, H. J. Fehling, and H.-R. Rodewald. 2005. Loss of histochemical identity in mast cells lacking carboxypeptidase A. *Mol. Cell. Biol.* 25: 6199–6210.

46. Jensen, B. M., P. M. Frandsen, E. M. Raaby, P. O. Schiøtz, P. S. Skov, and L. K. Poulsen. 2014. Molecular and stimulus-response profiles illustrate heterogeneity between peripheral and cord blood-derived human mast cells. *J. Leukoc. Biol.* 95: 893–901.

47. Ogasawara, T., M. Murakami, T. Suzuki-Nishimura, M. K. Uchida, and I. Kudo. 1997. Mouse bone marrow-derived mast cells undergo exocytosis, prostanoid generation, and cytokine expression in response to G protein-activating polybasic compounds after coculture with fibroblasts in the presence of c-kit ligand. *J. Immunol.* 158: 393–404.

48. Kowal, J., G. Arras, M. Colombo, M. Jouve, J. P. Morath, B. Primdal-Bengtson, F. Dingli, D. Loew, M. Tkach, and C. Théry. 2016. Proteomic comparison defines novel markers to characterize heterogeneous populations of extracellular vesicle subtypes. *Proc. Natl. Acad. Sci. USA* 113: E968–E977.

49. McNeil, B. D., P. Pundir, S. Meeker, L. Han, B. J. Undem, M. Kulka, and X. Dong. 2015. Identification of a mast-cell-specific receptor crucial for pseudo-allergic drug reactions. *Nature* 519: 237–241.

50. Trajkovic, K., C. Hsu, S. Chiantia, L. Rajendran, D. Wenzel, F. Wieland, P. Schwille, B. Brügger, and M. Simons. 2008. Ceramide triggers budding of exosome vesicles into multivesicular endosomes. *Science* 319: 1244–1247.

51. Möbius, W., E. van Donselaar, Y. Ohno-Iwashita, Y. Shimada, H. F. Heijnen, J. W. Slot, and H. J. Geuze. 2003. Recycling compartments and the internal vesicles of multivesicular bodies harbor most of the cholesterol found in the endocytic pathway. *Traffic* 4: 222–231.

52. Matsuo, H., J. Chevallier, N. Mayran, I. Le Blanc, C. Ferguson, J. Fauré, N. S. Blanc, S. Matile, J. Dubochet, R. Sadoul, et al. 2004. Role of LBPA and

53. Alix in multivesicular liposome formation and endosome organization. *Science* 303: 531–534.

54. Kobayashi, T., E. Stang, K. S. Fang, P. de Moerloose, R. G. Parton, and J. Gruenberg. 1998. A lipid associated with the antiphospholipid syndrome regulates endosome structure and function. *Nature* 392: 193–197.

55. Lin, D. A., and J. A. Boyce. 2006. Lysophospholipids as mediators of immunity. *Adv. Immunol.* 89: 141–167.

56. Gallala, H. D., and K. Sandhoff. 2011. Biological function of the cellular lipid BMP-BMP as a key activator for cholesterol sorting and membrane digestion. *Neurochem. Res.* 36: 1594–1600.

57. Kobayashi, T., U. M. Vischer, C. Rosnoblet, C. Lebrand, M. Lindsay, R. G. Parton, E. K. Kruithof, and J. Gruenberg. 2000. The tetraspanin CD63/lamp3 cycles between endocytic and secretory compartments in human endothelial cells. *Mol. Biol. Cell* 11: 1829–1843.

58. Goldstein, S. M., C. E. Kaempfer, J. T. Kealey, and B. U. Wintroub. 1989. Human mast cell carboxypeptidase. Purification and characterization. *J. Clin. Invest.* 83: 1630–1636.

59. Webber, J., R. Steadman, M. D. Mason, Z. Tabi, and A. Clayton. 2010. Cancer exosomes trigger fibroblast to myofibroblast differentiation. *Cancer Res.* 70: 9621–9630.

60. Vega, V. L., M. Rodríguez-Silva, T. Frey, M. Gehrmann, J. C. Diaz, C. Steinem, G. Multhoff, N. Arispe, and A. De Maio. 2008. Hsp70 translocates into the plasma membrane after stress and is released into the extracellular environment in a membrane-associated form that activates macrophages. *J. Immunol.* 180: 4299–4307.

61. Kunder, C. A., A. L. St John, G. Li, K. W. Leong, H. Berwin, H. F. Staats, and S. N. Abraham. 2009. Mast cell-derived particles deliver peripheral signals to remote lymph nodes. *J. Exp. Med.* 206: 2455–2467.

62. Savina, A., C. M. Fader, M. T. Damiani, and M. I. Colombo. 2005. Rab11 promotes docking and fusion of multivesicular bodies in a calcium-dependent manner. *Traffic* 6: 131–143.

63. Savina, A., M. Furlán, M. Vidal, and M. I. Colombo. 2003. Exosome release is regulated by a calcium-dependent mechanism in K562 cells. *J. Biol. Chem.* 278: 20083–20090.

64. Kalesnikoff, J., and S. J. Galli. 2008. New developments in mast cell biology. *Nat. Immunol.* 9: 1215–1223.

65. Peters, P. J., J. Borst, V. Oorschot, M. Fukuda, O. Krähenbühl, J. Tschopp, J. W. Slot, and H. J. Geuze. 1991. Cytotoxic T lymphocyte granules are secretory lysosomes, containing both perforin and granzymes. *J. Exp. Med.* 173: 1099–1109.

66. Peters, P. J., H. J. Geuze, H. A. Van der Donk, J. W. Slot, J. M. Griffith, N. J. Stam, H. C. Clevers, and J. Borst. 1989. Molecules relevant for T cell-target cell interaction are present in cytolytic granules of human T lymphocytes. *Eur. J. Immunol.* 19: 1469–1475.

67. Köberle, M., S. Kaesler, W. Kempf, F. Wölbing, and T. Biedermann. 2012. Tetraspanins in mast cells. *Front. Immunol.* 3: 106 doi:10.3389/fimmu.2012.00106.

68. Baietti, M. F., Z. Zhang, E. Mortier, A. Melchior, G. Degeest, A. Geeraerts, Y. Ivarsson, F. Depoortere, C. Coomans, E. Vermeiren, et al. 2012. Syndecan-syntenin-ALIX regulates the biogenesis of exosomes. *Nat. Cell Biol.* 14: 677–685.

69. Hsu, C., Y. Morohashi, S. Yoshimura, N. Manrique-Hoyos, S. Jung, M. A. Lauterbach, M. Bakhti, M. Grønborg, W. Möbius, J. Rhee, et al. 2010. Regulation of exosome secretion by Rab35 and its GTPase-activating proteins TBC1D10A-C. *J. Cell Biol.* 189: 223–232.

70. Kobayashi, T., M. H. Beuchat, M. Lindsay, S. Frias, R. D. Palmiter, H. Sakuraba, R. G. Parton, and J. Gruenberg. 1999. Late endosomal membranes rich in lysobisphosphatidic acid regulate cholesterol transport. *Nat. Cell Biol.* 1: 113–118.

71. Frederick, T. E., J. N. Chebukati, C. E. Mair, P. C. Goff, and G. E. Fanucci. 2009. Bis(monoacylglycero)phosphate forms stable small lamellar vesicle structures: insights into vesicular body formation in endosomes. *Biophys. J.* 96: 1847–1855.

72. Kalra, H., R. J. Simpson, H. Ji, E. Aikawa, P. Altevogt, P. Askenase, V. C. Bond, F. E. Borràs, X. Breakefield, V. Budnik, et al. 2012. Vesiclepedia: a compendium for extracellular vesicles with continuous community annotation. *PLoS Biol.* 10: e1001450.

73. Goldstein, S. M., J. Leong, L. B. Schwartz, and D. Cooke. 1992. Protease composition of exocytosed human skin mast cell protease-proteoglycan complexes. Tryptase resides in a complex distinct from chymase and carboxypeptidase. *J. Immunol.* 148: 2475–2482.

74. Trivedi, N. N., and G. H. Caughey. 2010. Mast cell peptidases: chameleons of innate immunity and host defense. *Am. J. Respir. Cell Mol. Biol.* 42: 257–267.

75. Afonina, I. S., C. Müller, S. J. Martin, and R. Beyaert. 2015. Proteolytic processing of interleukin-1 family cytokines: variations on a common theme. *Immunity* 42: 991–1004.

76. Reynolds, D. S., D. S. Gurley, R. L. Stevens, D. J. Sugarbaker, K. F. Austen, and W. E. Serafin. 1989. Cloning of cDNAs that encode human mast cell carboxypeptidase A, and comparison of the protein with mouse mast cell carboxypeptidase A and rat pancreatic carboxypeptidases. *Proc. Natl. Acad. Sci. USA* 86: 9480–9484.